ISBN: 978-3-95450-234-9 ISSN: 2673-5504 doi:10.18429/JACoW-SRF2023-MOPMB043

CHARACTERIZATION OF DISSIPATIVE REGIONS OF AN N-DOPED SRF CAVITY*

E. M. Lechner[1,†], B. D. Oli, M. Iavarone, Temple University, Philadelphia, PA, USA
J. Makita, A. Gurevich, Old Dominion University, Norfolk, VA, USA
G. Ciovati[2], Thomas Jefferson National Accelerator Facility, Newport News, VA, USA
[1]also at Thomas Jefferson National Accelerator Facility, Newport News, VA, USA
[2]also at Old Dominion University, Norfolk, VA, USA

Abstract

We report scanning tunneling microscopy measurements on N-doped cavity hot and cold spot cutouts. Analysis of the electron tunneling spectra using a proximity effect theory shows that hot spots have a reduced superconducting gap and a wider distribution of the contact resistance. Alone, these degraded superconducting properties account for a much weaker excess dissipation as compared with the vortex contribution. Based on the correlation between the quasiparticle density of states and temperature mapping, we suggest that degraded superconducting properties may facilitate vortex nucleation or settling of trapped flux during cooling the cavity through the critical temperature.

INTRODUCTION

Doping SRF cavities with impurities has been an effective method of producing Nb resonators with very high quality factors at moderate accelerating fields [1–8]. Performance of SRF cavities is inherently multifaceted. Towards gaining a deeper understanding of the mechanisms by which N-doping affects RF performance, accessing the quasiparticle density of states (DOS) is of great interest [9]. The DOS of surface of a superconductor can be examined in a straightforward manner by measuring the differential conductance via electron tunneling, dI/dV. In tunneling experiments that utilize a normal metal counter electrode the differential conductance reflects the DOS of the sample by Eq. (1) [10]

$$\frac{dI}{dV} \propto -\int_{-\infty}^{\infty} \frac{\partial f(\epsilon + eV)}{\partial V} N(\epsilon) d\epsilon, \qquad (1)$$

where f is the Fermi-Dirac distribution function, ϵ is the quasiparticle energy, V is the electric potential and N is the DOS of the sample. In the low temperature limit the differential conductance probes directly the density of states in the material of interest. Point contact spectroscopy and low temperature scanning tunneling microscopy and spectroscopy (STM/STS) have been used recently to investigate Nb cavity cutouts [11, 12]. These studies have revealed changes in $N(\epsilon)$ in the first few nm at the surface of Nb cavities after N-doping [11, 12]. It was shown that N-doping shrinks the metallic suboxide layer and reduces lateral inhomogeneities of the superconducting gap Δ and the contact resistance R_B between the suboxide and the Nb matrix, making R_B closer to an optimum value which minimizes R_s [12, 13]. At the same time, N-doping slightly reduces Δ at the surface [11, 12]. Here we identify hot and cold spots via temperature mapping of an SRF cavity and study their DOS via scanning tunneling microscopy.

EXPERIMENTAL

The cavity measured in this work was fabricated from ingot Nb from Tokyo Denkai, Japan, with residual resistivity ratio (RRR) of ~ 300 and large grains with size of a few cm^2. The cavity shape is that of the center cell of TESLA/EXFEL cavities [14]. Prior to N-doping, the cavity underwent standard buffered chemical polishing (BCP) and high pressure rinsing (HPR) with ultra-pure water. The cavity was N-doped by heating to 800 °C and exposing the cavity to a 25 mTorr nitrogen atmosphere for 30 minutes. After, the nitrogen was pumped-out and the cavity remained at 800 °C for 30 minutes, after which the furnace cooled naturally back to room temperature. Ultimately, ~ 10 µm were removed from the cavity's inner surface by electropolishing, followed by HPR, assembly in a clean room and evacuation on a vertical test stand. The temperature mapping system was attached to the outer cavity surface prior to insertion into a vertical test cryostat at Jefferson Lab [15].

The cavity performance, shown in Fig. 1, was limited in both tests by a quench at B_p ~ 88 mT, without any field emission. The first test was performed after cooling with liquid He with a cool-down rate of ~1.5 K/min when the temperature at the bottom of the cavity crossed the critical temperature. The second test was performed after warming up the cavity to 80 K followed by a cool-down at a faster rate of ~5 K/min. The higher Q_0 in Test 2 compared to that of Test 1 is due to a lower residual resistance, decreasing from 3.4 nΩ to 2.4 nΩ. This reduction of R_i resulting from a faster cooling rate is related to better expulsion of the residual ambient magnetic field inside the cryostat [16], B_a, which was ~0.2 µT during the experiments. Taking the difference of $1/Q(B_a)$ curves for these two tests we extract the additional surface resistance ΔR caused by the slower cooling rate. As shown in the inset in Fig. 1, ΔR_s is practically independent of B_a, thus extra vortices trapped at a lower cooling rate do not produce additional nonlinearity in $R_s(B_a)$ in this field range. $Q_0(T_0)$ was also measured between 1.6 – 2.1 K and 1 – 15 mT after the second cool-down. The temperature maps measured just below the quench field are shown in Fig. 2. The quench location was the same in

* Work supported by DE-AC05- 06OR23177
† lechner@jlab.org

ISBN: 978-3-95450-234-9 ISSN: 2673-5504 doi:10.18429/JACoW-SRF2023-MOPMB043

both tests, at sensor No. 10 at the azimuthal angle of 230° which is ~2 cm away from the equatorial weld, in the high magnetic field region of the cavity. The samples that were cut for this study are highlighted in white and labelled C,D and G on the temperature maps.

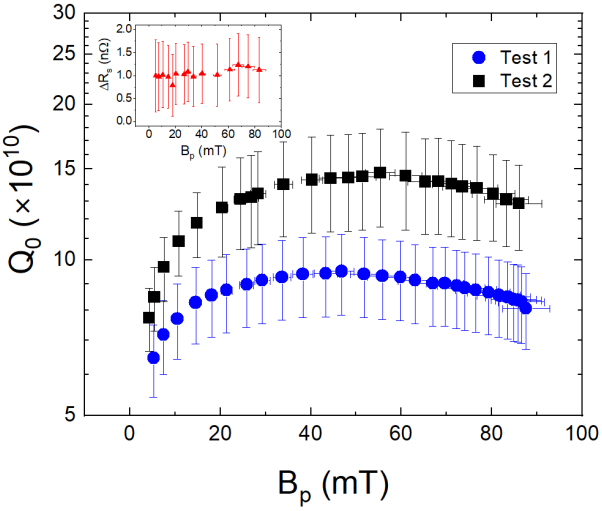

Figure 1: $Q_0(B_p)$ measured at 1.6 K after ~1.5 K/min (Test 1) and ~5 K/min (Test 2) cool-down rates across T_c. The inset shows the R_s-difference between Test 1 and Test 2 as a function of B_p.

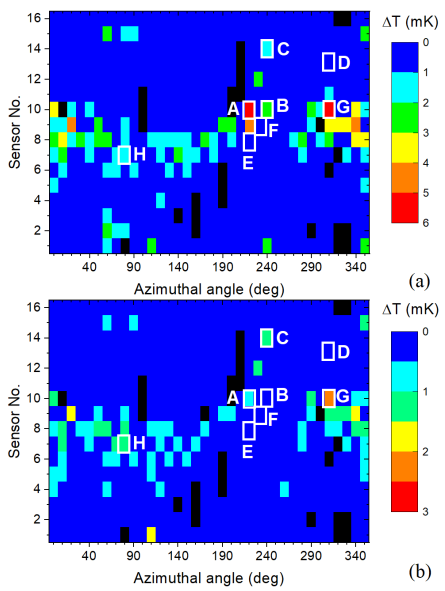

Figure 2: Unfolded temperature maps measured at 1.6 K and Bp ~ 84 mT during Test 1 (a) and Test 2 (b) before quench. Sensor No. 8 is at the equator, No. 1 is at the bottom iris and No. 16 at the top beam tube, close to the iris. The location of the cut-out samples, labelled A-H are highlighted in white. Faulty sensor locations are shown in black.

Cold and hot spot samples examined in this work were cut out from the same N-doped 1.3 GHz Nb superconducting cavity. A Unisoku ultra-high vacuum STM system equipped with a 9 T superconducting magnet and with a base pressure of 4×10^{-11} Torr was used to perform low temperature scanning tunneling microscopy/spectroscopy (STM/STS) measurements between 1.0 K to 1.5 K. Pt-Ir tips prepared on Au were used in all measurements. The samples used for STM measurements are cold (Sample D) and hot (Sample C and G) spot cutouts from the same N-doped Nb cavity. Since the surface of Nb is dominated by a layer of a dielectric oxide Nb_2O_5, which is too thick to tunnel through, it is necessary to remove the dielectric layer by Ar ion sputtering. These samples were sputter-cleaned in a UHV sample preparation chamber attached to the STM chamber with a base pressure of low 10^{-11} Torr. Ar ion sputtering was performed using 99.999% pure Ar at a pressure of 10^{-5} Torr and accelerating voltage of 1 kV for 1 hour with a 4.75 µA beam current and 10 mm × 10 mm beam size. The removal rate was 0.27 nm/min as estimated by atomic force microscopy on a calibration sample. The Ar sputtering process removes the surface pentoxide and yields a thin metallic oxide surface. This surface can be studied by STM that allows to study the local superconducting properties of the material. All (dI/dV) measurements were made with the same tunneling parameters. The junction was stabilized at $V = 10$ mV, $I = 60$ pA and a standard lock-in technique was used with $V_{mod} = 200\,\mu$V at 373.1 Hz. Tunneling conductance spectra were acquired with a spacing of 32.6 nm.

Representative tunneling spectra for sample C (cold spot) and sample D (hot spot) are shown in Fig. 3(a) and (b) respectively. The proximity effect theory, plotted in red in Fig. 3(a) and (b) accounts well for the shape of the conductance spectra which cannot be adequately fit using the Dynes model.

Calculation of the density of states at the surface of a normal layer proximity-coupled to a semi-infinite superconductor follows the work of Gurevich and Kubo [13] where the $\theta-$parameterization of the Usadel equations is used

$$N_N = N_n \Re\left[\frac{\cosh\theta_0 - i\beta\tilde{\epsilon}}{\sqrt{1-\beta^2\tilde{\epsilon}^2 - 2i\beta\tilde{\epsilon}\cosh\theta_0}}\right]. \quad (2)$$

Here $\tilde{\epsilon} = \epsilon + i\Gamma$ and Γ is the phenomenological Dynes scattering parameter. α, defined by $\alpha = \frac{dN_n}{\xi_s N_s}$, quantifies the effect of the normal layer and β, defined by $\beta = \frac{4e^2}{\hbar} R_B N_n \Delta d$, quantifies the interface transparency. The normal layer thickness is represented by d, N_n is the density of states in the normal layer, N_s is the density of states in the superconductor, and ξ_s is the coherence length in the superconductor. θ_0 is solved for via the self-consistency equation,

$$2k_\epsilon \sinh\frac{\theta_0 - \theta_\infty}{2} = i\tilde{\epsilon}\Phi\sinh\theta_0 + i\Psi\cosh\theta_0, \quad (3)$$

where

$$\Phi = \frac{\alpha}{\sqrt{1-\beta^2\tilde{\epsilon}^2 - 2i\beta\tilde{\epsilon}\cosh\theta_0}} \quad (4)$$

ISBN: 978-3-95450-234-9 ISSN: 2673-5504 doi:10.18429/JACoW-SRF2023-MOPMB043

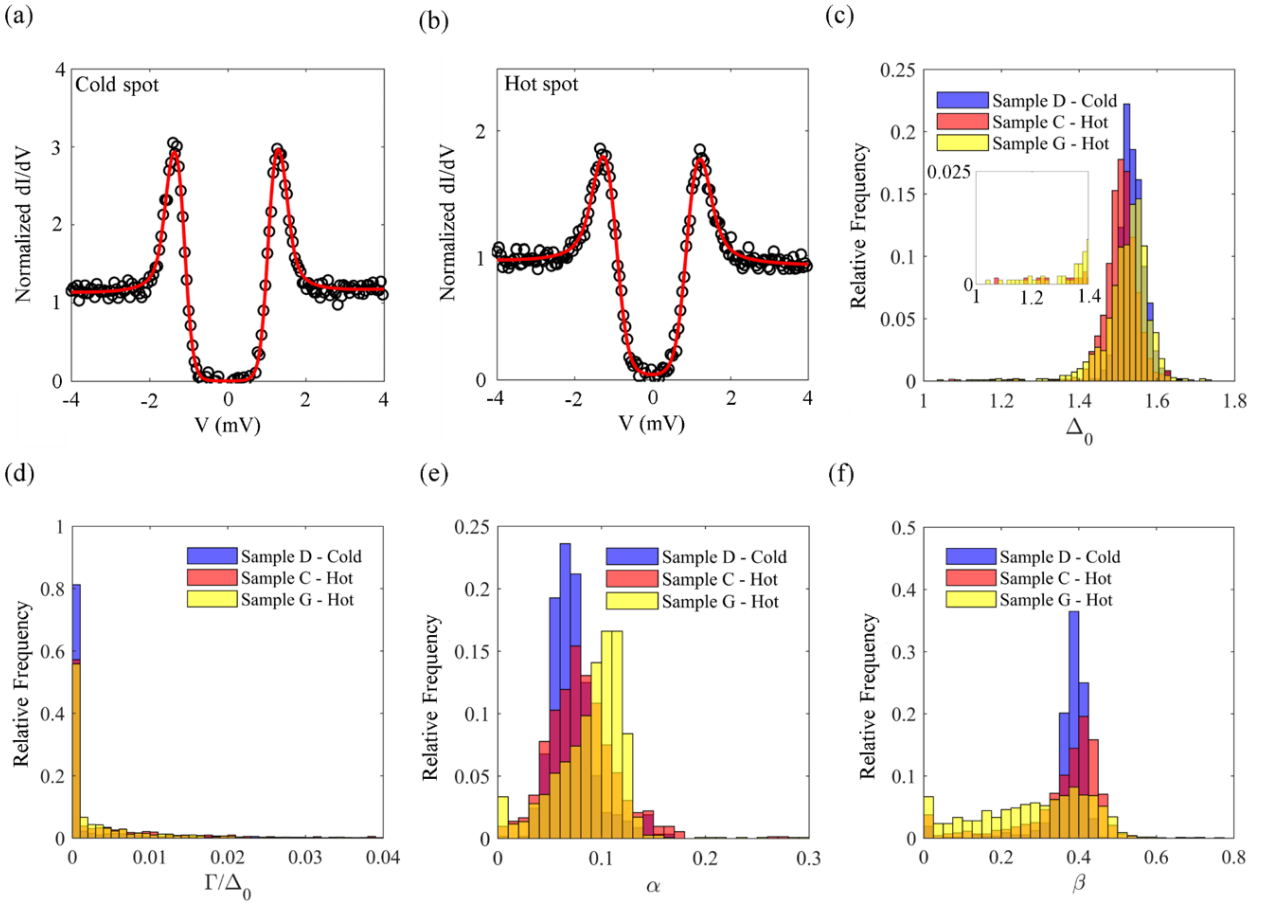

Figure 3: (a)-(b) Representative spectra for cold spot sample D and hot spot sample C from a N-doped Nb cavity. The red curves are the fit obtained using the proximity effect theory [13] and described in the text. The fitting parameters in (a) are: $\Delta_0 = 1.56$ meV, $\Gamma = 0$ meV, $\alpha = 0.08$, $\beta = 0.39$, $T = 1.17$ K. The fitting parameters in (b) are: $\Delta_0 = 1.51$ meV, $\Gamma = 0.03$ meV, $\alpha = 0.14$, $\beta = 0.04$, $T = 1.45$ K . The results of the fitting procedure for all tunneling spectra acquired on cold and hot spot samples between 1.0 K and 1.5 K are summarized in the histogram comparison for the fit parameters Δ_0 =, Γ/Δ_0, α, and β reported in (c)-(f). In panel (c) the low Δ_0 values are shown magnified by a factor 10 to better visualize the difference between cold and hot spot results.

$$\Psi = \frac{\alpha(\beta-1)}{1+\beta^2} + \frac{\alpha}{(1+\beta^2)^{\frac{3}{2}}} \ln \frac{(1+\beta\Lambda)(\beta+\sqrt{1+\beta^2})}{\sqrt{(1+\Lambda^2)(1+\beta^2)}-\Lambda+\beta}. \quad (5)$$

Here $\Lambda = \hbar\Omega/\Delta$, Ω is the Debye frequency and $\sinh\theta_\infty = \Delta/\sqrt{\tilde{\epsilon}^2-\Delta^2}$. In the limit of $\Gamma \ll \Delta$, $\Delta = \Delta_0 - \Gamma$.

Analysis of these spectra shows that the average Δ_0 is lower by 1% – 2% in the hot spot samples compared to the cold spot one. Furthermore, histograms of the extracted fit parameters clearly show that hot spots have wider distributions of α, β, Γ, Δ_0 than the cold spot. For instance, there is a low Δ_0 tail in the gap distribution in sample G, as shown in Fig. 3(c), where the low Δ_0 values have been magnified to show the difference between cold and hot spots. The number of tunneling spectra acquired for sample D was 576, that for sample C was 720 and that of sample G was 1108. The Dynes broadening parameter Γ is found to be higher, on average, in the hot spot samples as supported by the wider distribution for samples C and G, presented in Fig. 3(d). The α-distribution, shown in Fig. 3(e) reveals that hot spots are more likely to have larger normal layers which tend to be detrimental and enhance the surface resistance [1, 13]. The parameter β (Fig. 3(f)) in sample G exhibits a significant spread away from an optimum value of 0.3-0.4 at which a minimum in the surface resistance is predicted to occur [13].

CALCULATIONS OF LOW-FIELD R_s

With the parameters α, β, Γ and Δ_0 obtained from fitting the STM data $R_s(T)$ is calculated [13]. Additional parameters in the model are the electrons' mean free path, the resistivity of the normal layer, ρ_n, and the Debye energy, $\Lambda = 23.6$ meV, the latter taken as a material constant. $l = 6.2$ nm was obtained from a least-squares fit of $R_s(T_0)$ at 4.8 mT with $R_s(T) = R_{BCS}(T) + R_i$, where $R_{BCS}(T)$ is the low-field Mattis-Bardeen surface resistance calculated numerically with Halbritter's code [17]. $\lambda_0 = 32$ nm, $\xi_0 = 39$ nm and $T_c = 9.25$ K were considered material constants for clean Nb and the mean value $\overline{\Delta_0} = 1.536$ meV

ISBN: 978-3-95450-234-9 ISSN: 2673-5504 doi:10.18429/JACoW-SRF2023-MOPMB043

from cold-spot sample D was used in the numerical calculation. The overheating of the RF surface at 4.8 mT is very weak, such that $T_s \approx T_0$. Calculation of R_s proceeds according to the limit of a thin normal layer proximity-coupled to a semi-infinite superconductor [13].

$$R_s = \delta R + R_{s0}, \tag{6}$$

where δR quantities the surface resistance contribution from the normal layer via

$$\delta R = \frac{d}{\hbar}\int_{-\infty}^{\infty} \frac{\omega(e^{(\hbar\omega/k_BT)}-1)\mu_0{}^2\lambda^2\sigma_n}{(1+e^{(-\epsilon/k_BT)})(e^{(\epsilon+\hbar\omega)/k_BT}+1)} \times \left[n_N(\epsilon)n_N(\epsilon+\hbar\omega)+m_N(\epsilon)m_N(\epsilon+\hbar\omega)\right]d\epsilon \tag{7}$$

$$n_N(\epsilon) = \Re\left[\frac{\Delta\cosh\theta_0 - i\beta\tilde{\epsilon}}{\sqrt{\Delta^2-\beta^2\tilde{\epsilon}^2-2i\beta\tilde{\epsilon}\Delta\cosh\theta_0}}\right] \tag{8}$$

$$m_N(\epsilon) = \Re\left[\frac{\Delta\sinh\theta_0}{\sqrt{\Delta^2-\beta^2\tilde{\epsilon}^2-2i\beta\tilde{\epsilon}\Delta\cosh\theta_0}}\right] \tag{9}$$

and R_s quantities the surface resistance contribution from the superconductor via

$$R_s = \int_0^{\infty} dx \int_{-\infty}^{\infty} \frac{\omega(e^{(\hbar\omega/k_BT)}-1)\mu_0{}^2\lambda^2\sigma_s d\epsilon}{(1+e^{(-\epsilon/k_BT)})(e^{(\epsilon+\hbar\omega)/k_BT}+1)} \times \left[n_N(\epsilon)n_N(\epsilon+\hbar\omega)+m_N(\epsilon)m_N(\epsilon+\hbar\omega)\right]e^{-2x/\lambda} \tag{10}$$

$$n(\epsilon,x) = \Re\left[\frac{\tilde{\epsilon}(1+6t^2+t^4)+4t(1+t^2)\Delta}{(1-t^2)^2\sqrt{\tilde{\epsilon}^2-\Delta^2}}\right] \tag{11}$$

$$m(\epsilon,x) = \Re\left[\frac{(1+6t^2+t^4)\Delta+4\tilde{\epsilon}t(1+t^2)}{(1-t^2)^2\sqrt{\tilde{\epsilon}^2-\Delta^2}}\right] \tag{12}$$

$$t(x) = \tanh\left(\frac{\theta_0-\theta_\infty}{4}\right)e^{-k_\epsilon x/\xi_s}. \tag{13}$$

Here $k_\epsilon = (1-\tilde{\epsilon}^2/\Delta^2)^{1/4}$, ω is the cavity angular frequency and λ is the penetration depth in the superconductor.

The RF penetration depth and bulk coherence length used in the calculation of $R_s(T)$ with the proximity-coupled normal layer model were $\lambda = \lambda_0(1+0.88\xi_0/l)^{1/2} = 81.8$ nm and $\xi_s = 0.74\xi_0(1+0.88\xi_0/l)^{-1/2} = 11.3$ nm, respectively. ρ_n was used as a single fit parameter in the least-squares fit of the average cavity $R_s(T_0)$ measured 4.8 mT with $R_s(T)$ from the model. The average values $\overline{\alpha} = 0.0723$, $\overline{\beta} = 0.37$, $\overline{\Gamma} = 0.0051$ meV and $\overline{\Delta_0} = 1.536$ meV obtained from STM data on cold spot sample D were used in the numerical calculation of $R_s(T)$. The value of ρ_n from the fit was 0.5 μΩ cm and the calculated $R_s(T)$ is plotted in Fig. 4(a), showing a good agreement with the experimental data down to ~ 1.8 K. The deviation at lower temperature is indicative of an additional contribution to the residual resistance, other than that from the normal layer, such as that due to trapped vortices. The thickness of the normal layer, assuming $N_n \approx N_s$, is $d = \overline{\alpha}\xi_s = 0.8$ nm.

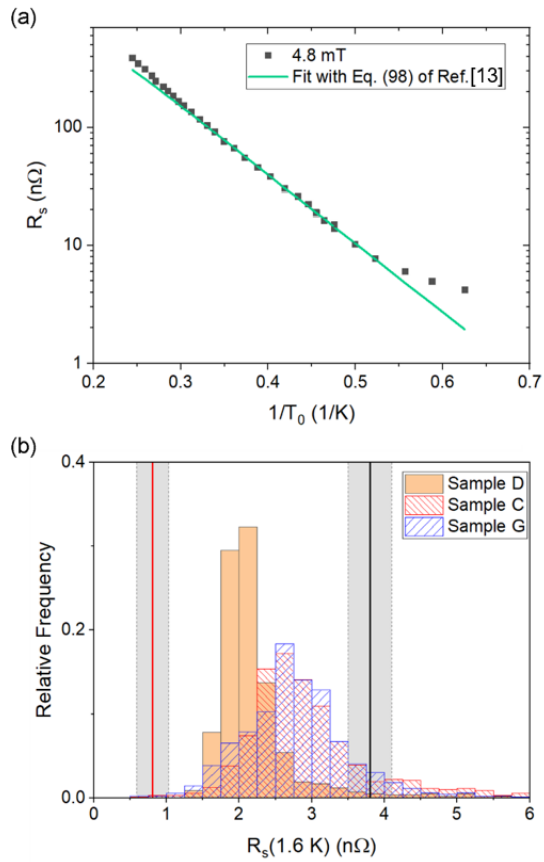

Figure 4: (a) Average cavity surface resistance as a function of LHe bath temperature, measured at 4.8 mT during Test 1 and $R_s(T)$ calculated with the model of Ref. [13] with the average parameters from cold spot D, $l = 6.2$ nm and $\rho_n = 0.5\,\mu\Omega$ cm. The size of the error bars are about the same size of the symbols. (b) Histograms of $R_s(1.6\text{ K})$ calculated with the model of Ref. [13] for each set of parameters α, β, Γ, Δ_0 from the STM data for samples C, D and G. The solid black line is $R_s(1.6\text{ K})$ measured during Test 2, the solid red line is $R_{BCS}(1.6\text{ K})$ and the gray shaded areas represent $\pm 1\sigma$.

CONCLUSION

Regions with different RF loss characteristics were located with thermometry mapping during the RF test of a N-doped Nb cavity. The cavity performance was limited by a quench at 86 mT and the quench location was the same after both slow and fast cooldown. A grain boundary was found at the quench location.

Cutouts from hot spot regions were characterized STM/STS measurements. The STM results can be described by a model which includes a thin proximity-coupled normal layer on top of the superconductor, resulting in small a degradation of both superconducting gap and degraded interface resistance in hot spot regions, compared to cold spot ones. The model parameters obtained from the STM measure-

ISBN: 978-3-95450-234-9 ISSN: 2673-5504 doi:10.18429/JACoW-SRF2023-MOPMB043

ments were used to calculate a distribution of R_s-values at 1.6 K. The thickness of the normal layer was estimated to be of the order of 1 nm, contributing by ~ 1.3 nΩ to the average residual resistance extracted from RF measurements.

Our analysis of the experimental data suggests that weakly degraded superconducting properties at the surface of hot spot regions are not the main source of RF losses, rather they are regions where vortices settle during cooldown. Vortex nucleation may also be preferential in theses locations but nucleation could also be facilitated by grain boundaries [18], such as found on samples A and G. While stronger thermal gradients will enhance flux expulsion as shown in Fig. 2, poorly superconducting regions remain vulnerable to preferentially trapping vortices.

ACKNOWLEDGEMENTS

This work was supported by the National Science Foundation, under award PHY-1734075. Some of the calculations were carried out on Temple University's HPC resources supported in part by the National Science Foundation through major research instrumentation grant N. 1625061 and by the US Army Research Laboratory under contract number W911NF-16-2-0189. G.C. is supported by Jefferson Science Associates, LLC under U.S. DOE Contract No. DE-AC05-06OR23177.

REFERENCES

[1] A. Grassellino *et al.*, "Nitrogen and argon doping of niobium for superconducting radio frequency cavities: A pathway to highly efficient accelerating structures", *Supercond. Sci. Technol.*, vol. 26, no. 10, p. 102 001, 2013. doi:10.1088/0953-2048/26/10/102001

[2] A. Romanenko, A. Grassellino, A. C. Crawford, D. A. Sergatskov, and O. Melnychuk, "Ultra-high quality factors in superconducting niobium cavities in ambient magnetic fields up to 190 mG", *Appl. Phys. Lett.*, vol. 105, no. 23, p. 234 103, 2014. doi:10.1063/1.4903808

[3] G. Ciovati, P. Dhakal, and A. Gurevich, "Decrease of the surface resistance in superconducting niobium resonator cavities by the microwave field", *Appl. Phys. Lett.*, vol. 104, no. 9, p. 092 601, 2014. doi:10.1063/1.4867339

[4] P. Dhakal *et al.*, "Effect of high temperature heat treatments on the quality factor of a large-grain superconducting radio-frequency niobium cavity", *Phys. Rev. Spec. Top. Accel. Beams*, vol. 16, p. 042 001, 4 2013. doi:10.1103/PhysRevSTAB.16.042001

[5] G. Ciovati, P. Dhakal, and G. R. Myneni, "Superconducting radio-frequency cavities made from medium and low-purity niobium ingots", *Supercond. Sci. Technol.*, vol. 29, no. 6, p. 064 002, 2016. doi:10.1088/0953-2048/29/6/064002

[6] J. T. Maniscalco, D. Gonnella, and M. Liepe, "The importance of the electron mean free path for superconducting radio-frequency cavities", *J. Appl. Phys.*, vol. 121, no. 4, p. 043 910, 2017. doi:10.1063/1.4974909

[7] S. Posen, A. Romanenko, A. Grassellino, O. Melnychuk, and D. Sergatskov, "Ultralow surface resistance via vacuum heat treatment of superconducting radio-frequency cavities", *Phys. Rev. Appl.*, vol. 13, p. 014 024, 1 2020. doi:10.1103/PhysRevApplied.13.014024

[8] E. M. Lechner, J. W. Angle, F. A. Stevie, M. J. Kelley, C. E. Reece, and A. D. Palczewski, "Rf surface resistance tuning of superconducting niobium via thermal diffusion of native oxide", *Appl. Phys. Lett.*, vol. 119, no. 8, p. 082 601, 2021. doi:10.1063/5.0059464

[9] A. Gurevich, "Tuning microwave losses in superconducting resonators", *Supercond. Sci. Technol.*, vol. 36, no. 6, p. 063 002, 2023. doi:10.1088/1361-6668/acc214

[10] E. L. Wolf, *Principles of electron tunneling spectroscopy*. OUP Oxford, 2011, vol. 152.

[11] N. Groll, G. Ciovati, A. Grassellino, A. Romanenko, J. Zasadzinski, and T. Proslier, "Insight into bulk niobium superconducting rf cavities performances by tunneling spectroscopy", 2018. doi:10.48550/arXiv.1805.06359

[12] E. M. Lechner, B. D. Oli, J. Makita, G. Ciovati, A. Gurevich, and M. Iavarone, "Electron tunneling and x-ray photoelectron spectroscopy studies of the superconducting properties of nitrogen-doped niobium resonator cavities", *Phys. Rev. Appl.*, vol. 13, p. 044 044, 4 2020. doi:10.1103/PhysRevApplied.13.044044

[13] A. Gurevich and T. Kubo, "Surface impedance and optimum surface resistance of a superconductor with an imperfect surface", *Phys. Rev. B*, vol. 96, p. 184 515, 18 2017. doi:10.1103/PhysRevB.96.184515

[14] B. Aune *et al.*, "Superconducting TESLA cavities", *Phys. Rev. Spec. Top. Accel. Beams*, vol. 3, p. 092 001, 9 2000. doi:10.1103/PhysRevSTAB.3.092001

[15] G. Ciovati, *Investigation of the superconducting properties of niobium radio-frequency cavities*. Old Dominion University, 2005.

[16] A. Romanenko, A. Grassellino, O. Melnychuk, and D. A. Sergatskov, "Dependence of the residual surface resistance of superconducting radio frequency cavities on the cooling dynamics around T_c", *J. Appl. Phys.*, vol. 115, no. 18, p. 184 903, 2014. doi:10.1063/1.4875655

[17] J. Halbritter, "FORTRAN-Program for the computation of the surface impedance of superconductors", Forschungszentrum Karlsruhe, Tech. Rep. FZK 3/70-6, 1970.

[18] S. Balachandran *et al.*, "Direct evidence of microstructure dependence of magnetic flux trapping in niobium", *Sci. Rep.*, vol. 11, no. 1, pp. 1–12, 2021. doi:10.1038/s41598-021-84498-x